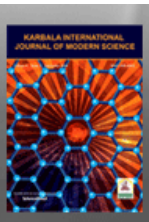

Karbala International Journal of Modern Science

Volume 10 | Issue 1 Article 3

The role of Cu (0-0.03) and Zn (0.02) substitution on the structural, optical and magnetic properties of MgO nanoparticles

S. Naseem Shah
Department of Physics, Federal Urdu University of Arts, Science and Technology, Karachi, Pakistan,,
syednaseemshah@fuuast.edu.pk

Atif Dawar
Department of Physics, Federal Urdu University of Arts, Science and Technology, Karachi, Pakistan,

Yasmeen Bibi
Department of Chemistry, Federal Urdu University of Arts, Science and Technology, Karachi, Pakistan

Abid Ali
Department of Biochemistry, Jinnah Sindh Medical University, Karachi, Pakistan.

M. Asif Siddiqui
Department of Physics, Federal Urdu University of Arts, Science and Technology, Karachi, Pakistan

Recommended Citation

Shah, S. Naseem; Dawar, Atif; Bibi, Yasmeen; Ali, Abid; and Siddiqui, M. Asif (2024) "The role of Cu (0-0.03) and Zn (0.02) substitution on the structural, optical and magnetic properties of MgO nanoparticles," *Karbala International Journal of Modern Science*: Vol. 10 : Iss. 1 , Article 3.
Available at: https://doi.org/10.33640/2405-609X.3335

The role of Cu (0-0.03) and Zn (0.02) substitution on the structural, optical and magnetic properties of MgO nanoparticles

Abstract

The co-precipitation method was employed to prepared Cu (0-0.03) and Zn (0.02) dual doped MgO nanoparticles. The secondary phases of CuO and Cu_2O were observed along with the cubical phase of MgO. The doping induced effect was noticed for the crystallite size variations (14.39-19.89 nm). The morphological transformation from spherical to rice-like shape were observed. The estimated values of optical bandgap (4.66-4.45 eV) were well correlated with the crystallite size and dopant concentrations. The ferromagnetic ordering was observed at room temperature and the enchantment in the coercivity (142.27 Oe) with Zn (0.02) doping was noticed. Such type of ferromagnetism at room temperature in the samples can be used for future multibit spintronic and data storage devices.

Keywords

Cu/Zn MgO; Size induced effect; Secondary phases; Bandgap; Ferromagnetism.

RESEARCH PAPER

The Role of Cu (0−0.03) and Zn (0.02) Substitution on the Structural, Optical and Magnetic Properties of MgO Nanoparticles

S. Naseem Shah [a,*], Atif Dawar [a], Yasmeen Bibi [b], Abid Ali [c], Muhammad Asif Siddiqui [a]

[a] Department of Physics, Federal Urdu University of Arts, Science and Technology, Karachi, Pakistan
[b] Department of Chemistry, Federal Urdu University of Arts, Science and Technology, Karachi, Pakistan
[c] Department of Biochemistry, Jinnah Sindh Medical University, Karachi, Pakistan

Abstract

The co-precipitation method was employed to prepared Cu (0−0.03) and Zn (0.02) dual doped MgO nanoparticles. The secondary phases of CuO and Cu_2O were observed along with the cubical phase of MgO. The doping induced effect was noticed for the crystallite size variations (14.39−19.89 nm). The morphological transformation from spherical to rice-like shape were observed. The estimated values of optical bandgap (4.66−4.45 eV) were well correlated with the crystallite size and dopant concentrations. The ferromagnetic ordering was observed at room temperature and the enchantment in the coercivity (142.27 Oe) with Zn (0.02) doping was noticed. Such type of ferromagnetism at room temperature in the samples can be used for future multibit spintronic and data storage devices.

Keywords: Cu/Zn MgO, Size induced effect, Secondary phases, Bandgap, Ferromagnetism

1. Introduction

Nanoparticles are extensively used in the industrial world due to their remarkable properties like optical, magnetic, electrical, structural, catalytic, corrosion, resistance etc. [1]. Among all metal oxides nanomaterials, MgO is an inorganic, thermally and chemically stable material having wide bandgap. This material is widely studied due to its unique properties in many applications such as optical coatings, water treatment, catalysis, fuel additives etc. [2]. MgO has flame retardant property due to which it is mostly used in crucible, refractive and coating materials [3−5].

The physical properties of metal oxides nanomaterials can be modulated significantly by adding the suitable dopant concentration in the host materials. It has been reported that the various element such as Cd, Fe, Zn, and Ca can be doped in MgO materials and these materials are widely used in optoelectronic application [6,7]. It has been studied that the doping of Mn in MgO changed the magnetic property of the materials from diamagnetic to ferromagnetic with increasing the dopant concentration [8]. The optical bandgap of MgO materials can be tuned from 3.37 to 7.8 eV with doping of Zn concentration [9]. Chayed NF et al. [10], studied that the doping of Cu (0, 0.05, 0.10) in MgO caused the reduction in the bandgap from 6.38 to 3.35 eV.

Apart from optical properties of this material, the magnetism in MgO thin film was also observed at room temperature [11]. It has been reported that the ferromagnetism induced in MgO films due the spinning of electron reflection in MgO lattice [12]. The studies showed that MgO capacitor have multilevel switching feature with ferromagnetism ordering and it can be used for data storage devices [13]. Recently, it was studied that MgO nanoparticles can be used to enhance oil production in the presence of magnetic field [14]. Such interesting features of this

Received 28 August 2023; revised 6 November 2023; accepted 8 November 2023.
Available online 23 January 2024

* Corresponding author.
E-mail address: syednaseemshah@fuuast.edu.pk (S. Naseem Shah).
Peer review under responsibility of University of Kerbala.

https://doi.org/10.33640/2405-609X.3335

materials compelled us to explore the structural, optical and magnetic properties. Therefore, it is very important to select suitable types of dopants and concentrations for tuning the optical and magnetic properties of MgO nanomaterials. In this study, we prepared the desired samples via low cost co-precipitation method to study the effect of Cu (0.01–0.03) and Zn (0.02) in MgO for modifying the structural, optical and magnetic properties.

2. Materials and methods

The cost effective co-precipitation method [15] was used for the preparation of the samples. In this chemical method, the NaOH was used as a precipitating agent to complete the reaction process with nitrate precursors of Mg, Zn and Cu as given in the following chemical equation (for pure MgO) [16].

$$Mg(NO_3)_2 + 2NaOH \rightarrow Mg(OH)_2 + 2NaNO_3$$

After completing the reaction process, the desired yield of the sample settles down and final product is obtained after removing unreacted product by washing several times with deionized water. The obtained sample is dried at 80 °C for 24 h and annealed at 400 °C for three hours to get pure MgO sample from $Mg(OH)_2$. The dual doping of Cu and Zn in MgO was carried out by varying the Cu concentrations from 0 to 0.03 while keeping fixed the concentration of Zn = 0.02. The following instruments were used in the lab for the samples preparation. (i) Digital Precision Balance: ATL: Max. 200G/Readability 0.001G, (ii) Hot plate with magnetic starrier, MS-300HS, temperature range 0–380 °C, speed range 0–1500 rpm (iii) Centrifuge machine 8000, max. speed 4000 rpm, Max. RSF 1790X9, Capacity 20 mL X 6, (iv) Furnace controller Box, SX-5-12 Box Resistance, max. temperature 200 °C (v) Thermostatic Drying Oven, DHG-920230L, max. temperature 1200 °C. The weighing of the metal precursor taken during the reaction process in gram as given in Table 1 along with samples IDs.

After the preparation of the samples, the following experimental techniques were used for the characterization of the samples. (i) X-ray diffractometer, X pert Pro, Model: DY 3313, Panalytical (Netherland), wavelength 0.154 nm (Cu Kα), (ii) Scanning electron microscope, JSM, Model: 6380A, JEOL (Japan), (iii) Energy Dispersive X-ray Spectroscopy, Model 6380A, equipped with SEM with accelerating voltage from 1 to 30 kV, (iv) UV/Vis spectrophotometer, Model: 730, Beckman Coulter, operating voltage is from 120 to 240 V, (v) Fourier Transform Infrared Spectroscopy, Model: 21, PerkinElmer FTIR.

Table 1. The values of the precursor weight in gram and samples ID.

Samples	Sample ID	$Mg(NO_3)_2$ $6H_2O$ (g)	$Cu(NO_3)_2$ $3H_2O$ (g)
$Mg_{0.98}Zn_{0.02}O$	C0Z2M	12.564	0.00
$Mg_{0.97}Cu_{0.01}Zn_{0.02}O$	C1Z2M	12.436	0.121
$Mg_{0.96}Cu_{0.02}Zn_{0.02}O$	C2Z2M	12.308	0.242
$Mg_{0.95}Cu_{0.03}Zn_{0.02}O$	C3Z2M	12.179	0.362

3. Results and discussion

3.1. XRD analysis

XRD spectra of Cu and Zn dual doped MgO nanostructures are shown in Fig. 1. The sharps and intense peaks clearly showed the high quality of crystals are present in the samples. The diffraction peaks associated with planes (1 1 1), (0 0 2), (2 0 2), (1 1 3) and (2 2 2) confirmed the formation of the cubical structure of MgO crystal lattice. These diffraction results were confirmed from JCPDS database card No. (30–0794) [17]. The phase purity of the samples is maintained to the certain limit of the dopant concentrations. The XRD spectra

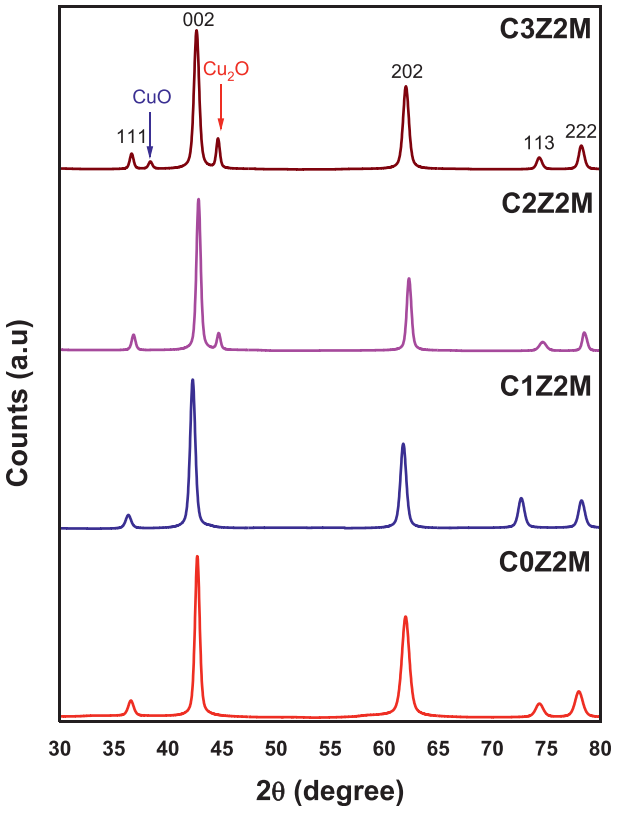

Fig. 1. XRD results of MgO nanostructures dually doped by Cu and Zn.

indicated that an additional peak at 2θ = 44.7° is observed for higher dopant concentration of Cu = 0.02 and this peak corresponds to the formation of Cu_2O in the samples. Furthermore, it is noticed that one more peak of CuO at 2θ = 38.4° is observed along with the peak of Cu_2O for increasing the Cu concentration from 0.02 to onward. It has been studied that such type of phase formation of CuO and Cu_2O was also observed in Fe-doped CuO samples [18]. Our results revealed that the formation of secondary phases started for $0.02 \leq Cu \leq 0.03$ in Zn (0.02) doped MgO samples. This showed the solubility limit of the Cu concentration in Zn (0.02) doped MgO sample. Similar secondary phase was also reported for higher dopant concertation (0.02 & 0.03) of S in ZnO nano-rods [19].

The average crystallite size was estimated from two sharp peaks by using the Scherrer formula [20]. The estimated size was found to increase from 14.39 to 19.89 nm with increasing Cu concentration up to 2 %. This increase in the crystallite size is due to the slightly greater ionic radius of Cu as compared to the Mg ionic radius [21]. The crystallite size is found to be decreased from the 19.89 to 15.55 nm due the formation two secondary phases of CuO and Cu_2O in the system. The similar effects were also reported for Mo alloys in which the secondary phases strongly influenced the size of the crystal lattice [22].

The values of crystallize size, lattice parameters and volume are calculated from the two sharps peaks associated to 2θ values, full width half maximum (FWHM) and d-values as shown in Table 2. The size variation in the samples are well correlated with dopant concentrations and the secondary phase formation of the crystal structures. The non-monotonically variations in the lattice parameters and volume of the crystals confirmed the successful doping of Zn and Cu in the host materials. These variations in the results are due to micro-strain produced in the crystals as reported in the case of Al doped ZnO-GO nanocomposites [23].

3.2. Morphology and elemental analysis

The results obtained from SEM and EDX of MgO nanostructures doped by Cu and Zn are shown in Fig. 2. The results indicated that all the particles are homogenous, uniformly distributed and these structures are within the nanometer range. The images belong to the C0Z2M and C1Z2M samples showed the spherical morphology approximately. On the other hand, the morphology of the sample is changed into rice like shape for higher concentration of $0.02 \leq Cu \leq 0.03$. This clearly indicates that the growth mode of crystal structures change with increasing the dopant concentration in the host materials up to the certain limit. The observed morphology of sample is (i) spherical shape due to the presence of the excess amount of OH^{-1} ions during the reaction process for low doping concentrations and (ii) rice-like shape due to the acidic nature by adding more amount of $Cu(NO_3)_2$ for higher dopant concentrations [24]. The expected values of the elemental mass present in the samples are very close to the experimental values as shown in Table 3.

3.3. UV–vis spectrum of the samples

The UV–Vis spectra of Cu (0.01–0.03) and Zn (0.02) dual doped MgO samples are shown in Fig. 3. The absorption spectra of these samples clearly indicated the slight shifting of the absorbance towards lower values of the wavelength for the higher dopant concentrations. The broadening in the absorption peaks is also observed for varying the dopant concentration in the host materials.

This shifting and broadening in the absorption peaks of the samples are due the defects produced by introducing the impurities in the system. The change in the crystallite size of the particles is also responsible for such shifting and broadening in the absorption spectra [25]. This type of changing in the absorption spectra is due to electronic transitions of Cu^{+2} and Zn^{+2} ions present in cubical structures of

Table 2. The average values of lattice parameter and size estimated from 2θ, FWHM, d values and Miller indices.

Sample ID	Lattice parameter (nm)	Volume $(nm)^3$	Size (nm)	2θ-values (degree)	FWHM (degree)	d-values (A^o)	Miller Indices
C0Z2M	4.237223	76.075351	14.39	42.68747	0.492	2.11818	(002)
				61.92923	0.7872	1.49839	(202)
C1Z2M	4.264141	77.534443	15.53	42.25981	0.5412	2.13862	(002)
				61.71984	0.5904	1.50297	(202)
C2Z2M	4.222061	75.261611	19.89	42.80027	0.4428	2.11286	(002)
				62.25039	0.4428	1.49143	(202)
C3Z2M	4.237378	76.083699	15.55	42.64422	0.5412	2.12023	(002)
				61.99091	0.5904	1.49705	(202)

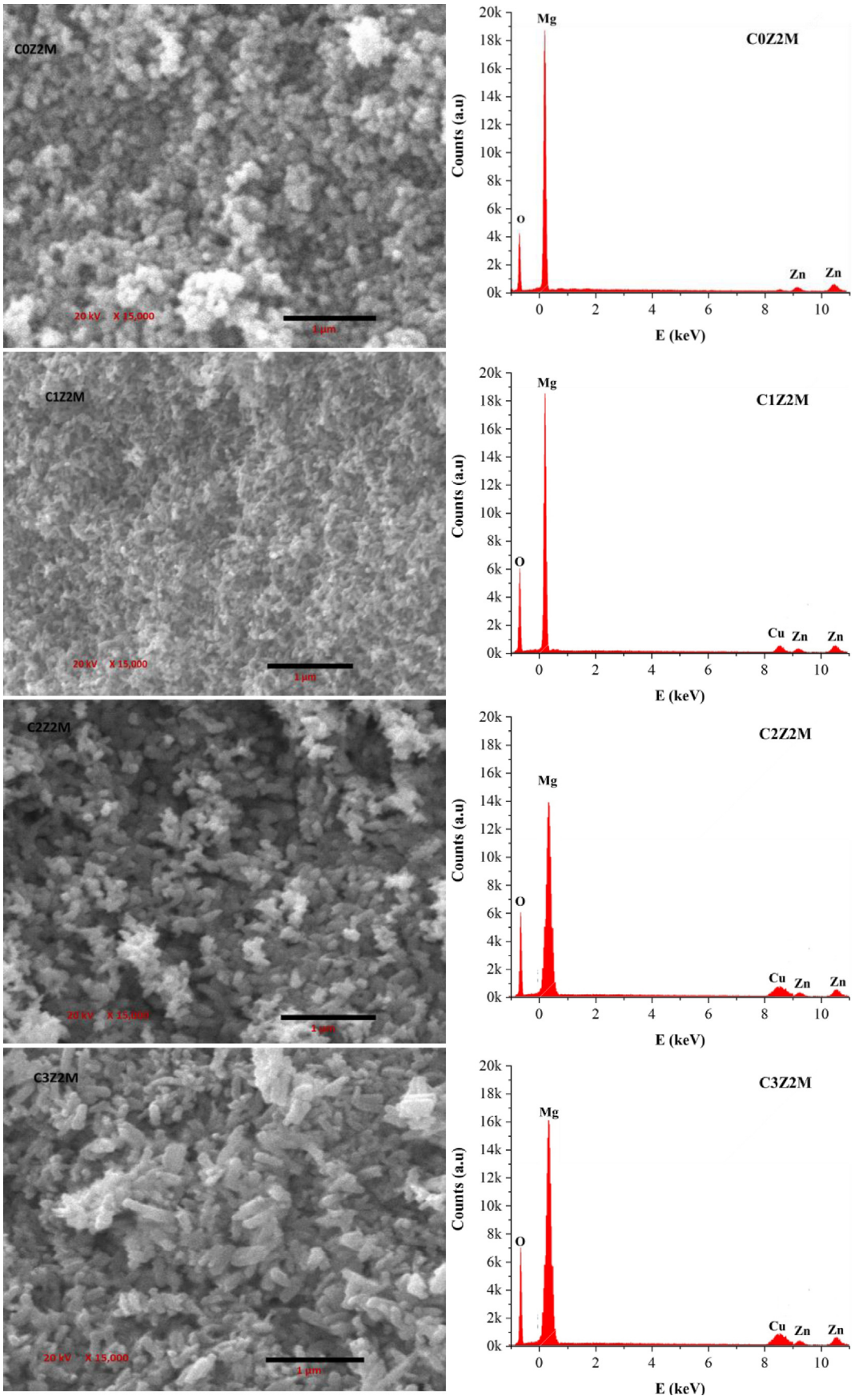

Fig. 2. SEM images and EDX results of MgO nanostructures dually doped by Cu and Zn.

Table 3. The expected and observed values of elemental mass for Cu (0.01–0.03)/Zn (0.02) dual doped MgO nanostructures.

Sample ID	Expected elemental mass %			Observed elemental mass %			
	Mg	Zn	Cu	Mg	Zn	Cu	O
C0Z2M	98	2	0	53.58	2.03	0	44.39
C1Z2M	97	2	1	51.23	1.98	1.02	45.77
C2Z2M	96	2	2	50.18	2.05	1.99	45.78
C3Z2M	95	2	3	48.39	2.02	2.95	46.64

the host materials [26]. Similar study is also reported for Mn/Co dual doping in ZnO samples [27]. Our samples showed the slight shifting in the UV region due to dopant concentrations and such types of nanomaterials can be used in broadband UV based devices [28].

The optical bandgap of the samples is estimated from the fitting of a straight line on the Tauc plot [29] as shown in Fig. 4. The estimated value of bandgap is found to be 4.66 eV for C0Z2M sample and these values decreased from 4.51 (for C1Z2M) to 4.45 eV (for C2Z2M). The decrease in the bandgap was observed for $0.01 \leq Cu \leq 0.02$ doped samples as compared to the Zn (0.02) doped sample which is

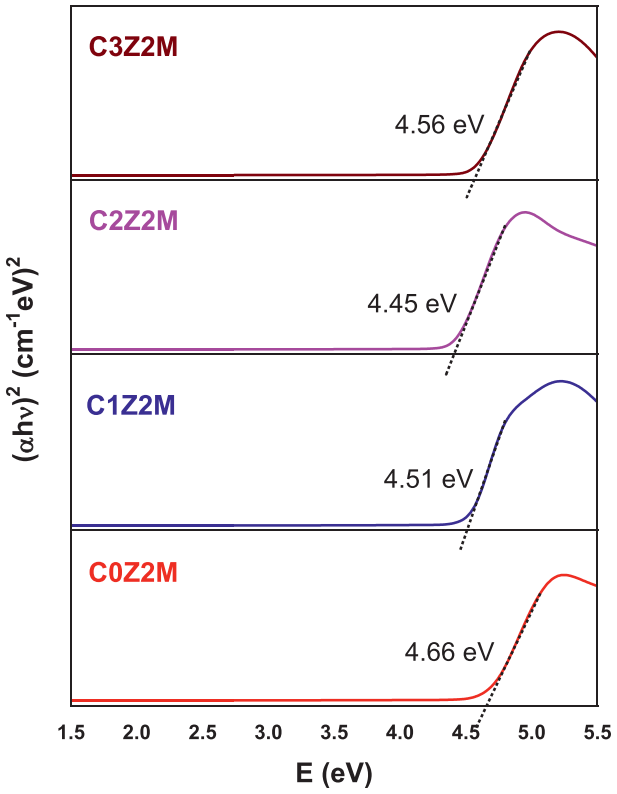

Fig. 4. Optical bandgap of Cu (0–0.03)/Zn (0.02) dual doped MgO nanostructures.

due to the certain amount of dopant concentration in MgO samples [30]. This decrease in the bandgap is due to incorporation of Zn^{+2} and Cu^{+2} ions in MgO structure and this amount of energy is enough to excite the electrons from the valance band to the conduction band [31]. Beside this, the enhancement in the optical bandgap (4.56 eV) is found for C3Z2M sample. This enhancement in the bandgap is due to the shift in the Fermi level towards the conduction band for higher dopant concentration in the host materials [32]. The variations in the optical bandgap

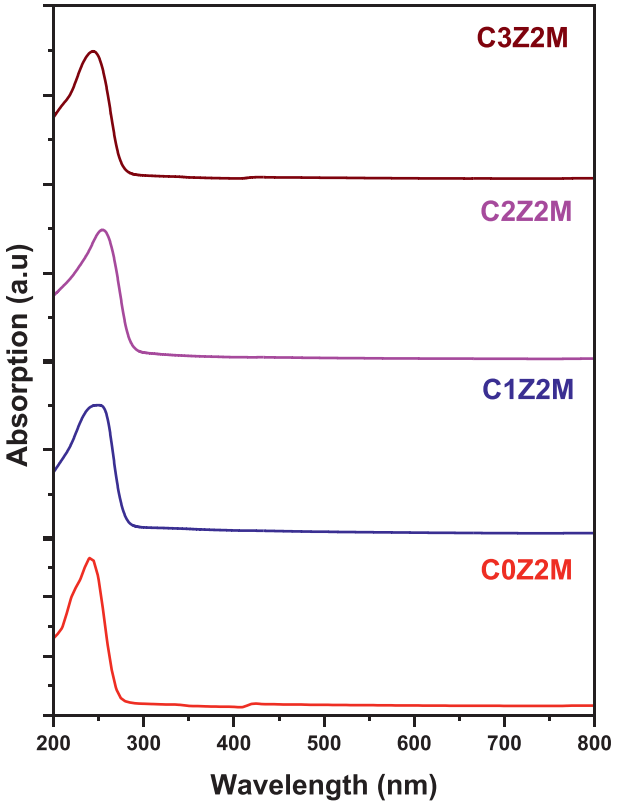

Fig. 3. Absorption spectra of Cu (0–0.03)/Zn (0.02) dual doped MgO nanostructures.

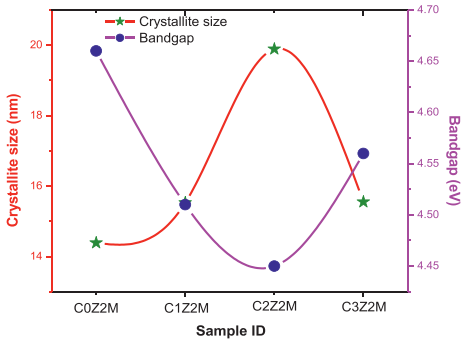

Fig. 5. The plot for the size and bandgap of Cu (0–0.03)/Zn (0.02) dual doped MgO nanostructures.

attributed due to the dopant concentration and size induced effect [33]. The graph is plotted between the crystallite size and the optical bandgap (see Fig. 5) which clearly indicated that the dopant concentrations, crystallite size and optical bandgap are strongly correlated to each other.

3.4. FTIR analysis

The FTIR spectra of Cu (0.01–0.03)/Zn (0.03) dual doped MgO samples in the range of 400–4000 cm^{-1} are shown in Fig. 6. The peak of vibration frequencies at 447 cm^{-1} and 449 cm^{-1} belong to the Mg–O molecule [34]. The broadening of this first peak is continued for increasing the dopant concentration. There is another spike close to the first peak appeared at 536 cm^{-1} for higher dopant concertation, which is due the presence of secondary phases (CuO and Cu_2O) in the samples [35,36]. The peaks at 1383 cm^{-1} and 1385 cm^{-1} are attributed the bending vibration of CO_3^{-2} ions due transparent matrix (KBr) used for sample preparation [37]. The small peak associated with the vibrational frequency varying from 1643 to 1653 cm^{-1} confirmed the presence of O–H bond, which is due to moisture absorbed by the sample during sample preparation for FTIR scanning [38]. Another broad peak varying from 3449 to 3455 cm^{-1} belong to O–H stretching, which is also due to moisture present in the atmosphere.

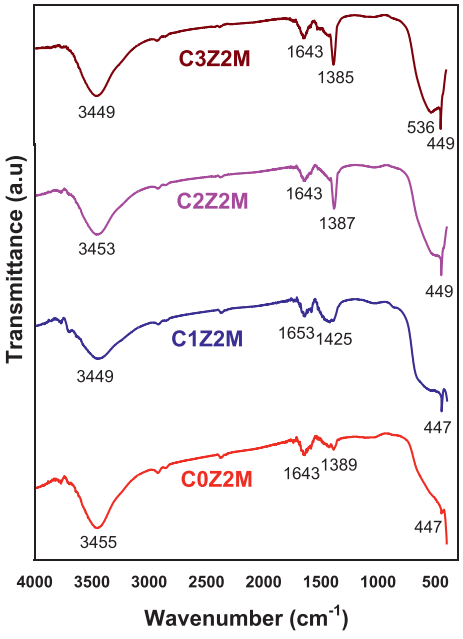

Fig. 6. FTIR spectra of Cu (0–0.03)/Zn (0.02) dual doped MgO nanostructures.

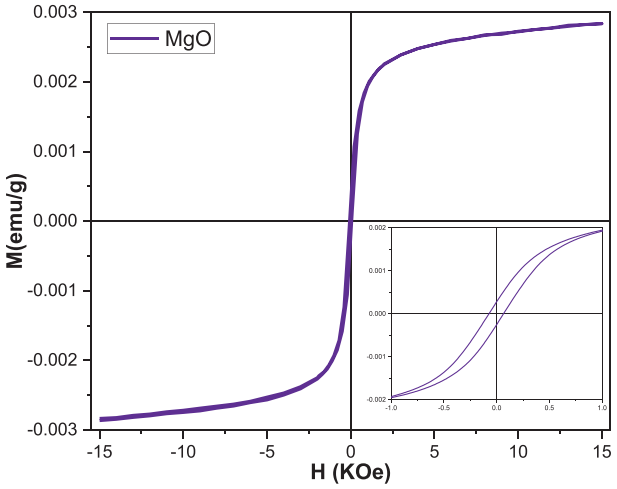

Fig. 7. VSM result of MgO nanostructures.

3.5. Magnetic properties

M–H loops are plotted for pure MgO (see Fig. 7) and Cu (0–0.03)/Zn (0.02) dual doped MgO nanostructures (see Fig. 8). The plotted data is recorded with the help of vibrating sample magnetometer (VSM) at room temperature for all samples. The small diamagnetism ordering is observed for all samples at the high field and it is subtracting from the recorded data using the standard method [39]. The inset in each graph clearly shows the different values for the magnetic moment (Ms), remnant magnetization (Mr) and coercivity (Hc). All samples showed d^o ferromagnetic ordering due to the empty d orbital of MgO [40]. All these estimated values and the ratio of oxygen to the concentrations are given in Table 4. The estimated values of Ms are varying from 0.0028 to 0.029 emu/g with respect to the doping concentrations. The magnetization for the MgO sample is found to be 0.0028 emu/g which confirmed the component of ferromagnetism present at the low field [41]. The origin of this ferromagnetism ordering is due to the presence of intrinsic defects in the sample at nanoscale level because observed formation energy at nanoscale is lower than the bulk MgO [42]. Studied shows that the Mg vacancy in the crystal lattice generated such types of magnetism in the MgO sample [43]. The magnetism in MgO nano-grain might be due to the presence of cation vacancies at the surface of the material [44]. The ferromagnetism ordering could also be due to both Mg and O vacancies in the crystal lattice. Theoretical study on the magnetism of MgO sample showed that vacancy in the lattice due to Mg can only be responsible for the spin polarization (2p) of oxygen electrons around the

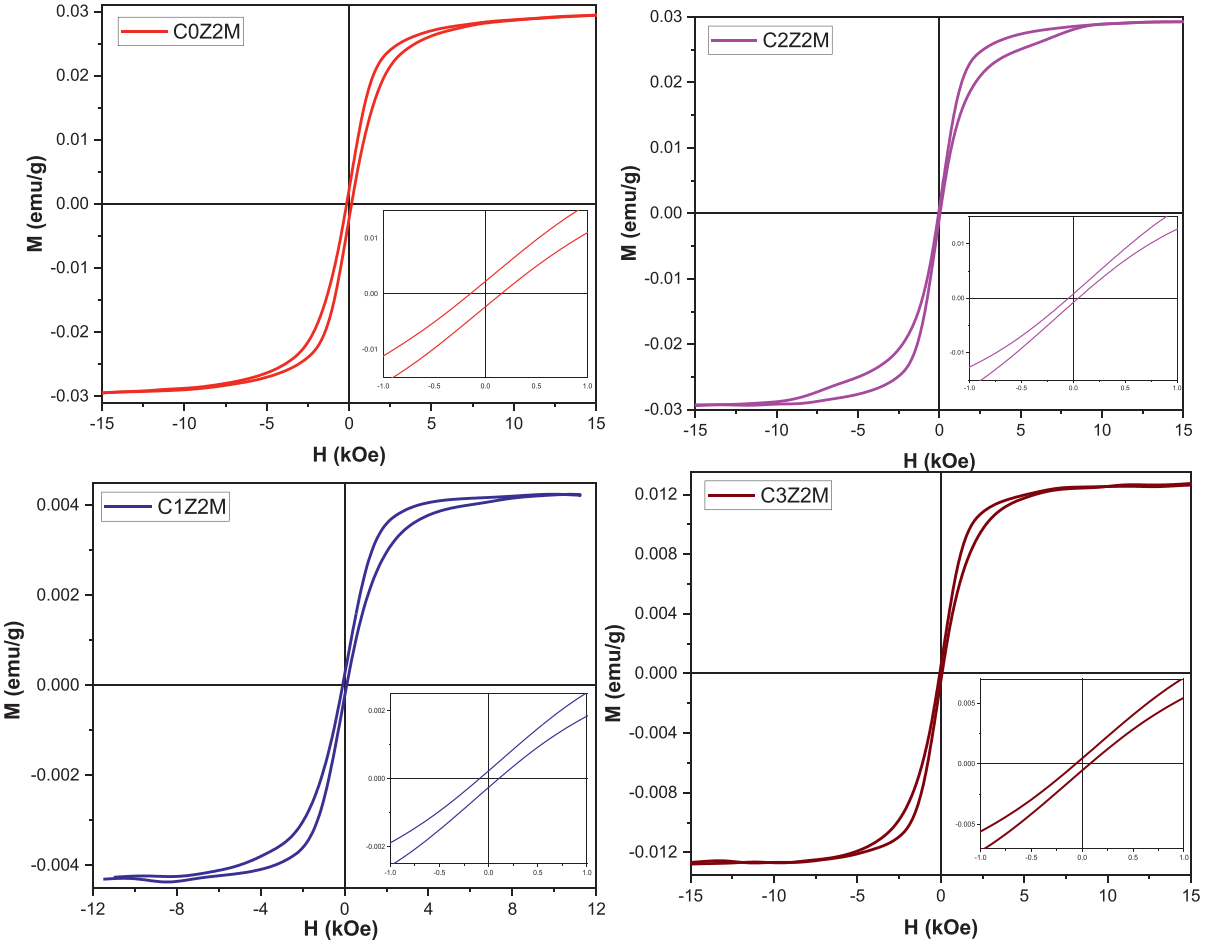

Fig. 8. VSM results of Cu (0–0.03)/Zn (0.02) dual doped MgO nanostructures.`

vacancy [42]. It is also noted that the coercivity of the sample first increased from 72.05 to 142.27 Oe with Zn (0.02) doping in MgO and then decreased with adding the concentration of Cu (0.01–0.03). Zeng et al., observed the same type of enhancement in coercivity for $MgFe_2O_4$ sample due to Zn doping [45]. It has been reported that the enhancement in magnetization and coercivity were due to exchange interaction between Zn^{+2} or Fe^{+3} and O^{-2} ions in the $MgFe_2O_4$ sample [46]. On the other side, the decrease in coercivity values are due to oxygen vacancies along with Cu impurities. It has been theoretically studied that the existence of the Cu atoms in the crystal lattice can change strongly the magnetic properties of the system [47,48]. The ferromagnetic ordering was also observed in Ni doped MgO due the existence of cation/anion vacancies in the crystal lattice [49]. Furthermore, it has been found that the oxides of Cu showed an antiferromagnetic ordering at 220 K temperature. Therefore, the secondary phases are responsible for the slight variation in the magnetic behavior of the samples for higher dopant concentration [50]. It is also observed that the M–H loop at higher field showed the linear trend due to non-interacting magnetic moment of the dopant. This trend in the result is in agreement with the defects produced in the system [51]. Therefore, our synthesized samples can be used for future multibit spintronic devices for data storage applications.

Table 4. The values of Ms, Mr, Hc and the ratio of oxygen to the concentrations.

Sample ID	Ms (emu/g)	Mr (emu/g)	Hc (Oe)	$\frac{[O]}{[Zn+Cu+Mg]}$
MgO	0.0028	2.80×10^{-4}	72.05	–
C0Z2M	0.0263	2.28×10^{-3}	142.27	0.80
C1Z2M	0.0042	2.38×10^{-4}	94.39	0.84
C2Z2M	0.02912	2.09×10^{-4}	51.53	0.85
C3Z2M	0.01256	4.84×10^{-4}	64.30	0.87

4. Conclusions

The structural, optical and magnetic properties were studied in Cu (0–0.03) and Zn (0.02) dual doped

MgO nanoparticles. The secondary phases of CuO and Cu_2O were observed for higher concentration of Cu along with the cubical phase of MgO lattice. The estimated crystallite size of the samples varied in accordance with the dopant concentrations. The morphology of the sample changed from spherical to rice-like shape with increasing the dopant concentrations. The EXD results showed that the experimental and expected elemental mass % present in the samples were in good agreement. There exists a strong correlation for optical bandgap with the crystallite size, morphology and formation of the secondary phases. The vibrational frequencies of the molecular bonds present in the samples were in accordance with the expected results. The M–H loop clearly indicated that the ferromagnetism ordering was present in all samples at the room temperature. The coercivity (142.27 Oe) of Zn (0.02) doped MgO sample was found to be larger than Cu doped samples. The results revealed that such nanomaterials can be used for future multibit spintronic devices for data storage applications.

Conflict of interest

The authors declare that they have no competing interests that could have appeared to influence the work reported in this paper.

Acknowledgements

The growth of samples was carried out at the Nanoscale condensed matter physics lab., Federal Urdu University of Arts, Science and Technology, Karachi, Pakistan. There is no external funding available for this work.

References

[1] K.G. Chandrappa, T.V. Venkatesha, Generation of nanostructured CuO by electrochemical method and its Zn–Ni–CuO composite thin films for corrosion protection, Mater. Corros. 64 (2013) 831–839, https://doi.org/10.1002/maco.201206767.

[2] W. Zhang, H.L. Tay, S.S. Lim, Y. Wang, Z. Zhong, R. Xu, Supported cobalt oxide on MgO: highly efficient catalysts for degradation of organic dyes in dilute solutions, Appl. Catal. B 95 (2010) 93–99, https://doi.org/10.1016/j.apcatb.2009.12.014.

[3] T. Selvamani, A. Sinhamahapatra, D. Bhattacharjya, I. Mukhopadhyay, Rectangular MgO microsheets with strong catalytic activity, Mater. Chem. Phys. 129 (2011) 853–861, https://doi.org/10.1016/j.matchemphys.2011.05.055.

[4] S. Suresh, D. Arivuoli, Synthesis and characterization of Pb^{+} doped MgO nanocrystalline particles, Digest J. Nanomater. Biostruct. 6 (2011) 1597–1603. https://www.researchgate.net/publication/267979017.

[5] B. Nagappa, G.T. Chandrappa, Mesoporous nanocrystalline magnesium oxide for environmental remediation, Microporous Mesoporous Mater. 106 (2007) 212–218, https://doi.org/10.1016/j.micromeso.2007.02.052.

[6] M. Silva, V. Murzin, L. Zhang, J. Baltrus, J. Baltrusaitis, Transition metal-doped MgO nanoparticles for nutrient recycling: an alternate Mg source for struvite synthesis from wastewater, Environ. Sci. Nano 7 (2020) 3482–3496, https://doi.org/10.1039/D0EN00660B.

[7] M.R. Anilkumar, H.P. Nagaswarupa, H. Nagabhushana, S.C. Sharma, Y.S. Vidya, K.S. Anantharaju, S.C. Prashantha, C. Shivakuamra, K. Gurushantha, Bio-inspired route for the synthesis of spherical shaped MgO: Fe^{3+} nanoparticles: structural, photoluminescence and photocatalytic investigation, Spectrochim. Acta A Mol. Biomol. Spectrosc. 149 (2015) 703–713, https://doi.org/10.1016/j.saa.2015.05.003.

[8] S. Azzaza, M. El-Hilo, S. Narayanan, J.J. Vijaya, N. Mamouni, A. Benyoussef, A. El Kenz, M. Bououdina, Structural, optical and magnetic characterizations of Mn-doped MgO nanoparticles, Mater. Chem. Phys. 143 (2014) 1500–1507, https://doi.org/10.1016/j.matchemphys.2013.12.006.

[9] V. Etacheri, R. Roshan, V. Kumar, Mg-doped ZnO nanoparticles for efficient sunlight-driven photocatalysis, ACS Appl. Mater. Interfaces 4 (2012) 2717–2725, https://doi.org/10.1021/am300359h.

[10] N.F. Chayed, N.O. Kamarulzaman, N.U. Badar, K.E. Elong, Effect of Cu doped in MgO on nanostructures and their band gap energies, Solid State Phenom. 290 (2019) 323–328, https://doi.org/10.4028/www.scientific.net/SSP.290.323.

[11] J.P. Singh, C.L. Chen, C.L. Dong, J. Prakash, D. Kabiraj, D. Kanjilal, W.F. Pong, K. Asokan, Role of surface and subsurface defects in MgO thin film: XANES and magnetic investigations, Superlattice Microstruct. 77 (2015) 313–324, https://doi.org/10.1016/j.spmi.2014.10.035.

[12] Y.Z. Wu, A.K. Schmid, Z.Q. Qiu, Spin-dependent quantum interference from epitaxial MgO thin films on Fe (001), Phys. Rev. Lett. 97 (2006) 217205, https://doi.org/10.1103/PhysRevLett.97.217205.

[13] O. Jambois, P. Carreras, A. Antony, J. Bertomeu, C. Martínez-Boubeta, Resistance switching in transparent magnetic MgO films, Solid State Commun. 151 (2011) 1856–1859, https://doi.org/10.1016/j.ssc.2011.10.009.

[14] F. Amrouche, M.J. Blunt, S. Iglauer, M. Short, T. Crosbie, E. Cordero, D. Xu, Using magnesium oxide nanoparticles in a magnetic field to enhance oil production from oil-wet carbonate reservoirs, Mater. Today Chem. 27 (2023) 101342, https://doi.org/10.1016/j.mtchem.2022.101342.

[15] G. Vaidyanathan, S. Sendhilnathan, Characterization of $Co_{1-x}Zn_xFe_2O_4$ nanoparticles synthesized by co-precipitation method, Phys. B: Condens. 403 (2008) 2157–2167, https://doi.org/10.1016/j.physb.2007.08.219.

[16] M.M. Imani, M. Safaei, Optimized synthesis of magnesium oxide nanoparticles as bactericidal agents, J. Nanotechnol. 1–6 (2019), https://doi.org/10.1155/2019/6063832.

[17] A.A. Hamead, F.M. Othman, M.A. Fakhri, Preparation of MgO–MnO_2 nanocomposite particles for cholesterol sensors, J. Mater. Sci. Mater. Electron. 32 (2021) 15523–15532, https://doi.org/10.1007/s10854-021-06102-2.

[18] G.M. Al-Senani, S.I. Al-Saeedi, N.S. Al-Kadhi, O.H. Abd-Elkader, N.M. Deraz, Green synthesis and pinning behavior of Fe-doped CuO/Cu_2O/Cu_4O_3 nanocomposites, Processes 10 (2022) 729, https://doi.org/10.3390/pr10040729.

[19] U.K. Panigrahi, M. Barik, S. Hussain, P.K. Satapathy, P. Mallick, Sulphur doping induced band gap narrowing and enhancement of green emission in ZnO nanorods, J. Mater. Sci. Mater. Electron. 33 (2022) 22851–22861, https://doi.org/10.1007/s10854-022-09053-4.

[20] R.S. Mohammed, K.A. Aadim, K.A. Ahmed, Synthesis of CuO/ZnO and MgO/ZnO core/shell nanoparticles with plasma jets and study of their structural and optical properties, Karbala Int. J. Mod. Sci. 8 (2022) 88–97, https://doi.org/10.33640/2405-609X.3225.

[21] L. Zheng, R. Lin, D. Luo, L. Guo, J. Zhang, Effect of Mg^{2+} additives on Nieuwland catalyst: the role of the second metal ionic radius, J. Chin. Chem. Soc. 69 (2022) 522–531, https://doi.org/10.1002/jccs.202100540.

[22] Z.Z. Wu, Z.H.A.O. Na, L.U. Yao, H.L. Liu, B.H. Duan, X.L. Liu, D.Z. Wang, Effects of shape and size of second phase on mechanical properties of sintered Mo-Y_2O_3 alloys, Trans. Nonferr. Met. Soc. China 32 (2022) 1926–1934, https://doi.org/10.1016/S1003-6326(22)65919-3.
[23] F. Ahmed, S. Kumar, N. Arshi, M.S. Anwar, B.H. Koo, Morphological evolution between nanorods to nanosheets and room temperature ferromagnetism of Fe-doped ZnO nanostructures, Cryst. Eng. Comm. 14 (2012) 4016–4026, https://doi.org/10.1039/C2CE25227A.
[24] T.A. Hameed, W. Sharmoukh, B. Anis, A.M. Youssef, Enhanced photocatalytic activity and diode performance of ZnO-GO nanocomposites via doping with aluminum, Int. J. Energy Res. 46 (2022) 22601–22624, https://doi.org/10.1002/er.8563.
[25] W.J. Qin, J. Sun, J. Yang, X.W. Du, Control of Cu-doping and optical properties of ZnO quantum dots by laser ablation of composite targets, Mater. Chem. Phys. 130 (2011) 425–430, https://doi.org/10.1016/j.matchemphys.2011.07.001.
[26] M.K. Patra, K. Manzoor, M. Manoth, S.R. Vadera, N. Kumar, Studies on structural and magnetic properties of Co-doped pyramidal ZnO nanorods synthesized by solution growth technique, J. Phys. Chem. Solids 70 (2009) 659–664, https://doi.org/10.1016/j.jpcs.2009.02.003.
[27] A. Safeen, K. Safeen, M. Shafique, Y. Iqbal, N. Ahmed, M.A. R. Khan, G. Asghar, K. Althubeiti, S. Al Otaibi, G. Ali, W.H. Shah, The effect of Mn and Co dual-doping on the structural, optical, dielectric and magnetic properties of ZnO nanostructures, RSC Adv. 12 (2022) 11923–11932, https://doi.org/10.1039/D2RA01798A.
[28] S.A. Khan, N.Z. Khan, N. Muhammad, F. Lin, M. Runowski, J. Ahmed, S. Agathopoulos, J. Li, Highly efficient and tunable broadband UV excitable $Ba_9Lu_2Si_6O_{24}$: Eu^{2+}, Mn^{2+} single-phase white-light-emitting phosphors, J. Alloys Compd. 938 (2023) 168650, https://doi.org/10.1016/j.jallcom.2022.168650.
[29] Y. Feng, S. Lin, S. Huang, S. Shrestha, G. Conibeer, Can Tauc plot extrapolation be used for direct-band-gap semiconductor nanocrystals? J. Appl. Phys. 117 (2015) 125701 https://doi.org/10.1063/1.4916090.
[30] C. Belkhaoui, N. Mzabi, H. Smaoui, P. Daniel, Enhancing the structural, optical and electrical properties of ZnO nanopowders through (Al^+ Mn) doping, Results Phys. 12 (2019) 1686–1696, https://doi.org/10.1016/j.rinp.2019.01.085.
[31] E. Pragna, M. Ramanadha, A. Sudharani, K.S. Kumar, Nano synthesis and characterization of Co and Mn co-doped ZnO by solution combustion technique, J. Supercond. Nov. Magn. 34 (2021) 1507–1516, https://doi.org/10.1007/s10948-021-05874-2.
[32] Y.H. Yang, X.Y. Chen, Y. Feng, G.W. Yang, Physical mechanism of blue-shift of UV luminescence of a single pencil-like ZnO nanowire, Nano Lett. 7 (2007) 3879–3883, https://doi.org/10.1021/nl071849h.
[33] C. Mrabet, O. Kamoun, A. Boukhachem, M. Amlouk, T. Manoubi, Some physical investigations on hexagonal-shaped nanorods of lanthanum-doped ZnO, J. Alloys Compd. 648 (2015) 826–837, https://doi.org/10.1016/j.jallcom.2015.07.009.
[34] H.A. Prescott, Z.J. Li, E. Kemnitz, J. Deutsch, H. Lieske, New magnesium oxide fluorides with hydroxy groups as catalysts for Michael additions, J. Mater. Chem. 15 (2005) 4616–4628, https://doi.org/10.1039/B510108E.
[35] Z.P. Hu, Y.P. Zhu, Z.M. Gao, G. Wang, Y. Liu, X. Liu, Z.Y. Yuan, CuO catalysts supported on activated red mud for efficient catalytic carbon monoxide oxidation, J. Chem. Eng. 302 (2016) 23–32, https://doi.org/10.1016/j.cej.2016.05.008.
[36] W. Yao, Y. Zhang, T. Duan, W. Zhu, Z. Yi, X. Cui, 3D hierarchical walnut-like CuO nanostructures: preparation, characterization and their efficient catalytic activity for CO oxidation, Phys. B: Condens. 493 (2016) 7–13, https://doi.org/10.1016/j.physb.2016.03.028.
[37] R. Kant, Y.K. Agarwal, K. Kumar, S. Bansal, S. Kaul, Superior dielectric behaviour and band gap tuning of Zn doped MgO nanoparticles, Mater. Technol. 37 (2022) 3017–3024, https://doi.org/10.1080/10667857.2022.2110795.
[38] M. Ashokkumar, S. Muthukumaran, Microstructure, optical and FTIR studies of Ni, Cu co-doped ZnO nanoparticles by co-precipitation method, Opt. Mater. 37 (2014) 671–678, https://doi.org/10.1016/j.optmat.2014.08.012.
[39] S. Phokha, J. Klinkaewnarong, S. Hunpratub, K. Boonserm, E. Swatsitang, S. Maensiri, Ferromagnetism in Fe-doped MgO nanoparticles, J. Mater. Sci. Mater. Electron. 27 (2016) 33–39, https://doi.org/10.1007/s10854-015-3713-9.
[40] J.P. Singh, K.H. Chae, d Ferromagnetism of magnesium oxide, Cond. Matter 2 (2017) 36, https://doi.org/10.3390/condmat2040036.
[41] J. Hu, Z. Zhang, M. Zhao, H. Qin, M. Jiang, Room-temperature ferromagnetism in MgO nanocrystalline powders, Appl. Phys. Lett. 93 (2008) 1–3, https://doi.org/10.1063/1.4793308.
[42] F. Wang, Z. Pang, L. Lin, S. Fang, Y. Dai, S. Han, Magnetism in undoped MgO studied by density functional theory, Phys. Rev. B 80 (2009) 144424, https://doi.org/10.1103/PhysRevB.80.144424.
[43] C. Martínez-Boubeta, J.I. Beltrán, L. Balcells, Z. Konstantinović, S. Valencia, D. Schmitz, J. Arbiol, S. Estrade, J. Cornil, B. Martínez, Ferromagnetism in transparent thin films of MgO, Phys. Rev. B 82 (2010) 1–7, https://doi.org/10.1103/PhysRevB.82.024405.
[44] P.B. Devaraja, D.N. Avadhani, H. Nagabhushana, S.C. Prashantha, S.C. Sharma, B.M. Nagabhushana, H.P. Nagaswarupa, B.D. Prasad, Luminescence properties of MgO: Fe^{3+} nanopowders for WLEDs under NUV excitation prepared via propellant combustion route, J. Radiat. Res. Appl. Sci. 8 (2015) 362–373. https://core.ac.uk/download/pdf/82150875.pdf.
[45] X. Zeng, Z. Hou, J. Ju, L. Gao, J. Zhang, Y. Peng, The cation distributions of Zn-doped normal spinel $MgFe_2O_4$ ferrite and its magnetic properties, Materials 15 (2022) 2422, https://doi.org/10.3390/ma15072422.
[46] G.D. Dwivedi, F. Tseng, L. Chan, S.L. Chatterjee, A.K. Ghosh, H.D. Yang, S. Chatterjee, Signature of ferroelectricity in magnetically ordered Mo-doped $CoFe_2O_4$, Phys. Rev. B 82 (2010) 134428, https://doi.org/10.1103/PhysRevB.82.134428.
[47] J.H. Yang, L.Y. Zhao, Y.J. Zhang, Y.X. Wang, H.L. Liu, M.B. Wei, Structure and magnetic properties of Mn-doped ZnO semiconductors, Solid State Commun. 143 (2007) 566–569, https://doi.org/10.1016/j.ssc.2007.06.033.
[48] K.S.K. Sato, H.K.Y.H. Katayama-Yoshida, Material design for transparent ferromagnets with ZnO-based magnetic semiconductors, Jpn. J. Appl. Phys. 39 (2000) 555, https://doi.org/10.1143/JJAP.39.L555.
[49] J. Narayan, S. Nori, D.K. Pandya, D.K. Avasthi, A.I. Smirnov, Defect dependent ferromagnetism in MgO doped with Ni and Co, Appl. Phys. Lett. 93 (2008) 082507, https://doi.org/10.1063/1.2977614, 082507.
[50] V. Ney, V. Venkataraman, F. Wilhelm, A. Rogalev, A. Ney, Structural and magnetic properties of Cu-doped ZnO epitaxial films at the coalescence limit - a superparamagnetic CuO-ZnO nanocomposite, J. Appl. Phys. 126 (2019) 143904, https://doi.org/10.1063/1.5124352.
[51] S.K. Satpathy, U.K. Panigrahi, S.K. Panda, R. Biswal, W. Luyten, P. Mallick, Structural, optical, antimicrobial and ferromagnetic properties of $Zn_{1-x}La_xO$ nanorods synthesized by chemical route, J. Alloys Compd. 865 (2021) 158937, https://doi.org/10.1016/j.jallcom.2021.158937.